Flow (2022), **1** E1
doi:?????

SUPPLEMENTARY INFORMATION

Vahid Nourian[1]* and Henry Shum[1]

[1]Department of Applied Mathematics, University of Waterloo, Waterloo, ON, N2L 3G1, Canada
*Corresponding author. E-mail: Vnourian@uwaterloo.ca

S1. Define the functions used in the boundary integral equations

$$J_1 = \frac{2\epsilon^2 + \|\vec{x}-\vec{\gamma}\|^2}{8\pi\mu(\|\vec{x}-\vec{\gamma}\|^2+\epsilon^2)^{3/2}}, \tag{1}$$

$$J_2 = \frac{1}{8\pi\mu(\|\vec{x}-\vec{\gamma}\|^2+\epsilon^2)^{3/2}}, \tag{2}$$

$$J_3 = \frac{1}{8\pi\mu\|\vec{x}-\vec{\Psi}\|}, \tag{3}$$

$$J_4 = \frac{1}{8\pi\mu\|\vec{x}-\vec{\Psi}\|^3}, \tag{4}$$

$$P_1 = \frac{5\epsilon^2 + 2\|\vec{x}-\vec{\gamma}\|^2}{8\pi\mu(\|\vec{x}-\vec{\gamma}\|^2+\epsilon^2)^{5/2}} \tag{5}$$

$$P_2 = \frac{1}{4\pi\mu\|\vec{x}-\vec{\Psi}\|^3}, \tag{6}$$

$$K_1 = \frac{10\epsilon^4 - 7\epsilon^2\|\vec{x}-\vec{\gamma}\|^2 - 2\|\vec{x}-\vec{\gamma}\|^4}{8\pi\mu(\|\vec{x}-\vec{\gamma}\|^2+\epsilon^2)^{7/2}}, \tag{7}$$

$$K_2 = \frac{21\epsilon^2 + 6\|\vec{x}-\vec{\gamma}\|^2}{8\pi\mu(\|\vec{x}-\vec{\gamma}\|^2+\epsilon^2)^{7/2}}. \tag{8}$$

S2. Iterative method to find rotor orientation

Each of the bacterial motors has a rotor, which rotates about the axis of the motor (also referred to as the rotor axis). To simplify notation in this section, we explain our model for a single flagellum and drop indices for distinguishing between the two flagella. The motor, which is embedded in the cell membrane of the bacterium, is assumed to be fixed in position and orientation with respect to the cell body. We define the orientation vectors of the flagellum $\vec{e}_1, \vec{e}_2, \vec{e}_3$, to be those of the rotor. The rotor axis is $\vec{e}_1$, which is fixed in the cell body frame, defined by the angles α and β. The transverse direction vectors $\vec{e}_2$ and $\vec{e}_3$ rotate about the rotor axis with a variable rotational speed W^{rot} that we calculate iteratively at each time step to be consistent with the prescribed motor torque.

The rotational motion of the rotor is transmitted to the filament via the bacterial hook segment. In our model, the rotor, hook, and filament are described by a single Kirchhoff rod discretized into segments of equal lengths. The zeroth segment of the rod represents the rotor, while the other segments constitute the hook and filament (we do not distinguish between hook and filament segments in this study). For the Kirchhoff rod description, we adopt the common convention that the third director, $\vec{D}_3$, is the tangential

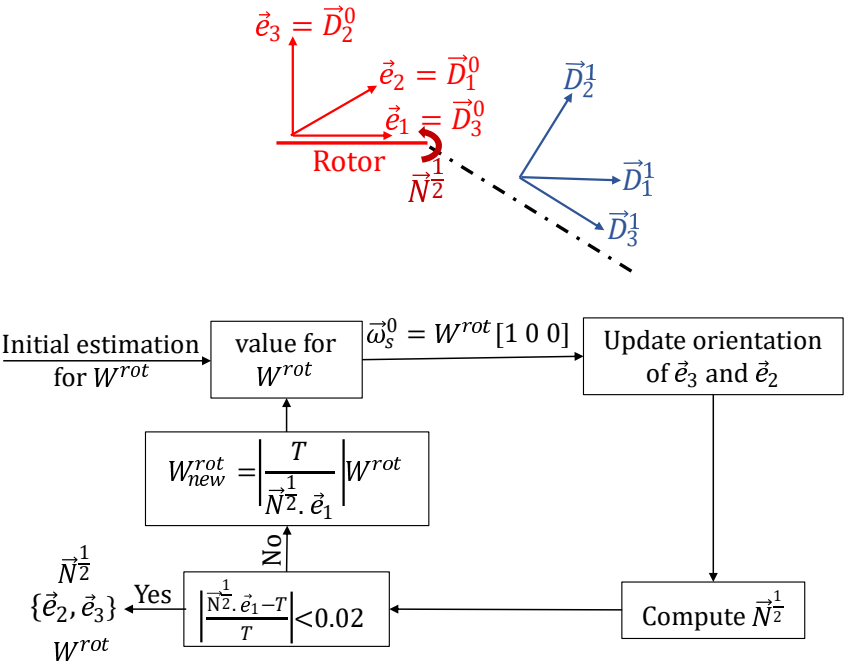

Figure S 1. *Flowchart of the iterative method to find the rotor orientation, the motor speed and the internal moment at the joint connects the flagellum to the rotor. The rotor and the corresponding triad are marked by red color and the first segment of flagellum is represented by dashed line.*

direction along the curve. Thus, we define the relationships for the rotor segment

$$\vec{D}_3^0 = \vec{e}_1, \quad \vec{D}_1^0 = \vec{e}_2, \quad \vec{D}_2^0 = \vec{e}_3. \tag{9}$$

At any given time, we assume that all positions and orientations of the segments are known. The angular velocities $\vec{\omega}_s^n, n = 1, 2, .., N_{\text{fl}}$, are determined by solving the system of linear equations described in the main text. The orientations of segments $n = 1, 2, ..., N_{\text{fl}}$ are determined at the next time step using an explicit time integration rule. The orientation of the rotor, however, is not updated in this manner because explicit time-stepping would generally not satisfy the motor torque constraint,

$$\vec{N}^{\frac{1}{2}} \cdot \vec{e}_1 = T, \tag{10}$$

where the torque transmitted from the rotor to the filament $\vec{N}^{\frac{1}{2}}$ depends on the directors at the zeroth and first segments of the rod according to the Kirchhoff rod model [equation (14) of the main text with $n = 0$]. Note that this motor torque condition prescribes only the component of torque in the axial direction. The other two components of torque are due to bending.

In our methodology, we use an iterative method to adjust $\vec{e}_2$ and $\vec{e}_3$ at each time step so that equation (10) is satisfied. We start with an initial trial value of the rotor angular velocity W^{rot} equal to its value at the previous time step. We next update $\vec{e}_2$ and $\vec{e}_3$ based on their values at the previous time step and the estimate for W^{rot}. Then, the projection of $\vec{N}^{\frac{1}{2}}$ onto $\vec{e}_1$ is compared with the target value of T. According to the obtained error, W^{rot} is adjusted and the iteration continues so that a desirable error for the motor torque constraint is achieved. The steps of this iterative method are presented schematically in figure S1.

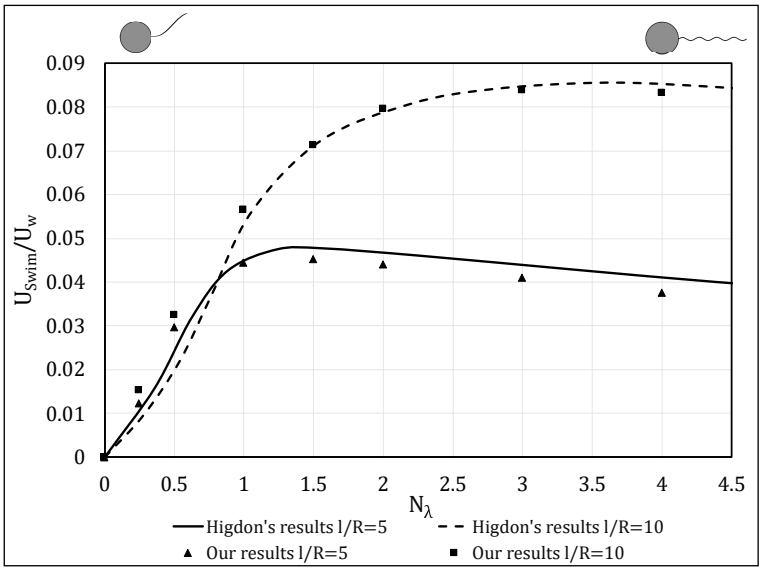

Figure S 2. *Comparison of the obtained results for swimming speed of a uni-flagellated bacterium with Higdon's. U_{swim}/U_w is the progressive speed non-dimensionalized by the linear wavespeed of the flagellum. R and l are the cell body radius and the flagellum length, respectively. N_λ represents the flagellum wavenumber.*

S3. Validation

We begin with a comparison of numerical results from our method with those obtained by Higdon [1979] to validate our boundary element method. In this test, we calculate the swimming speed of a model bacterium with a single rigid flagellum and a spherical cell body. The flagellum is divided into 30 and 60 segments for the shorter ($l/R = 5$) and longer ($l/R = 10$) flagellum, respectively, and we choose the other parameters according to the Higdon's model. As shown in figure S2, the swimming speeds of the model bacterium for two different flagellum lengths are in good agreement with the published results. To validate the elastic model, the equilibrium shape of a flexible filament settles in a viscous fluid is compared with an analytical solution derived by Xu and Nadim [1994] for the case of small deformation amplitudes. In particular, if it is assumed that a flexible filament with non-dimensional length 2 and a large bending modulus (3 in our test) settles horizontally under a uniform force, by applying the force correction factor the maximum non-dimensional deflection becomes about 0.07 and so the given solution is valid. If the filament is discretized into $n = 30$ segments, the relative l^2-norm of the deviation of the numerical displacements y^{num} from the analytical solution y^{an} evaluated at corresponding discrete points is $E_{l^2} = \sqrt{\sum_{j=1}^{n} |y_j^{\text{an}} - y_j^{\text{num}}|^2 / \sum_{j=1}^{n} |y_j^{\text{an}}|^2} \approx 0.022$. Since the deflection of the filament is small, the drag coefficient of the flexible filament should be comparable with a rigid straight rod in a viscous fluid ($C_N = 4\pi\mu l/(\ln(2l/d) - 0.5)$ (Cox [1970])). The minimum difference between the drag coefficients achieved in higher stiffnesses is about 3.8%. Such a difference is reasonable because our filament has finite length and a relatively large thickness whereas the mentioned formula is accurate only for very long and thin filaments. In the last step of the validation, it is verified that the swimming speed of a uni-flagellated bacterium with flexible flagellum converges to the rigid model as the stiffness of the flagellum increases. In particular if we consider Higdon's model bacterium with $N_\lambda = 1$ and $l/R = 5$, the swimming speeds of the model bacterium with flagellum stiffnesses $k_f = 3$, $k_f = 10$ and $k_f = 15$ are respectively 93.6%, 97.4% and 98.7% of the rigid model speed. It is worth mentioning that the swimming speeds of this model bacterium with a flexible flagellum are always lower than that with a rigid flagellum.

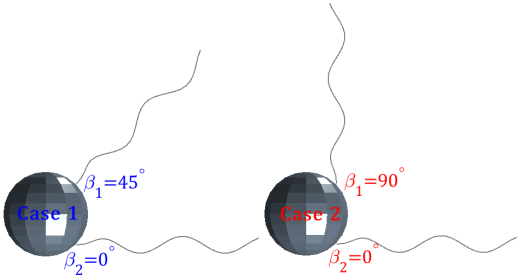

Figure S 3. *Model bacteria with two asymmetric pusher flagella*

S4. Swimming trajectory of pusher-pusher model bacterium

In addition to the puller-pusher configuration, pusher-pusher configurations of two flagella may also lead to double helical trajectories. Our simulations indicate that there is a correlation between the degree of the asymmetry (asymmetric cell body shape, flagella positions and orientations, the propulsive forces magnitude and orientations) and the properties of the large helices. In the studied puller-pusher model bacteria, the rest configurations are almost symmetrical but the differences in the magnitude and orientations of two propulsive forces (one for the pusher flagellum and one for the puller one) induce a torque on the cell body that leads to the rotation of the cell body in the directions other than its spinning. In fact, this rotation is responsible for the appearance of the second (large) helix.

In a pusher-pusher model bacterium with symmetrical configuration, the average effective torque induced by the propulsive forces on the cell body is near zero and therefore the bacterium moves on a single helical trajectory, as shown in Fig. 3. The second (larger) helix appears in the trajectory of the pusher-pusher model bacterium as the rest configuration of the model bacterium is geometrically asymmetrical. To quantitatively compare the properties of the trajectories in puller-pusher and pusher-pusher model bacteria, we have plotted the trajectories of two pusher-pusher model bacteria with different degrees of asymmetry (Figure S3) in Figure S4. The properties of both model bacteria are as stated in Table S1 and only the orientation of the first flagellum distinguishes Case 1 from Case 2. As expected, the size of the large helix increases by the degree of the asymmetry. Our measurements indicate that the pitch and diameter of the large helix in Case 1 (less-symmetrical) are 2.52 and 0.15, respectively, whereas they are 3.71 and 0.26, respectively, in Case 2. Comparing these values with the closest case in the puller-pusher configuration (pitch: 3.91 and diameter: 1.08) demonstrates that the amplitude of the large helix is several times smaller in the pusher-pusher configuration. This difference is likely due to the bundling effect of the two pusher flagella; flexible flagella have a tendency to bend towards each other, reducing the degree of the asymmetry in the pusher-pusher configuration and therefore causes the bacterium to swim smoothly on a smaller helix.

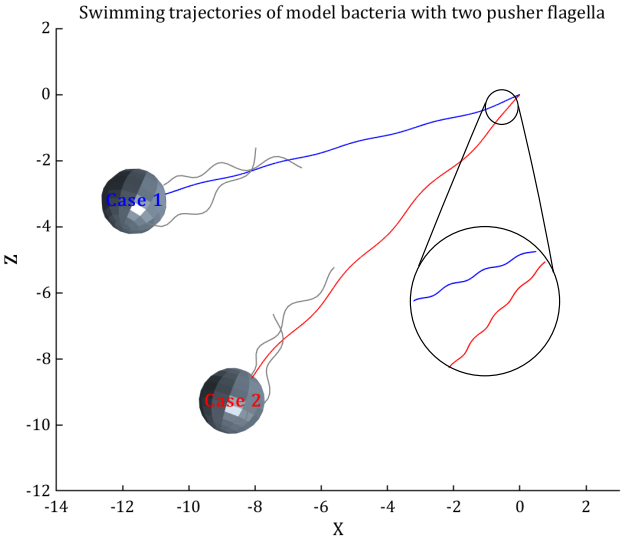

Figure S 4. *Trajectories of the model bacteria with two asymmetric pusher flagella*

Table S 1. *Parameters defining the shape of the model bacterium and simulation settings.*

Description	Symbol	Dimensionless Value	Dimensional Value
Radius of cell body	R	1	0.65 µm
Flagella diameter	d	0.1	65 nm
Each filament total length	l	5	3.25 µm
Flagella rest/initial pitch	p	2	1.3 µm
Flagella rest/initial amplitude	a	0.2	0.13 µm
Amplitude growth factor	k_E	2	4.73 μm^{-1}
Flagella relative stiffness (Flexural rigidity)	$k_f\ (EI)$	1	(7.8 pN μm^2)
Number of segments on each flagellum	N_{fl}	30	30
Number of triangular elements on the cell body	N_{head}	112	112
Pusher flagellum motor torque in $\vec{e}_1^{(1)}$ direction	T_1	-1	-12 pN µm
Puller flagellum motor torque in $\vec{e}_1^{(2)}$ direction	T_2	1	12 pN µm
Flagella rest/initial orientation (rotor orientation) with respect to $\vec{e}_1^{(B)}$	β	45°	45°
Motor position with respect to $\vec{e}_1^{(B)}$	α	45°	45°
Total swimming time	T_s	1000	0.023 s

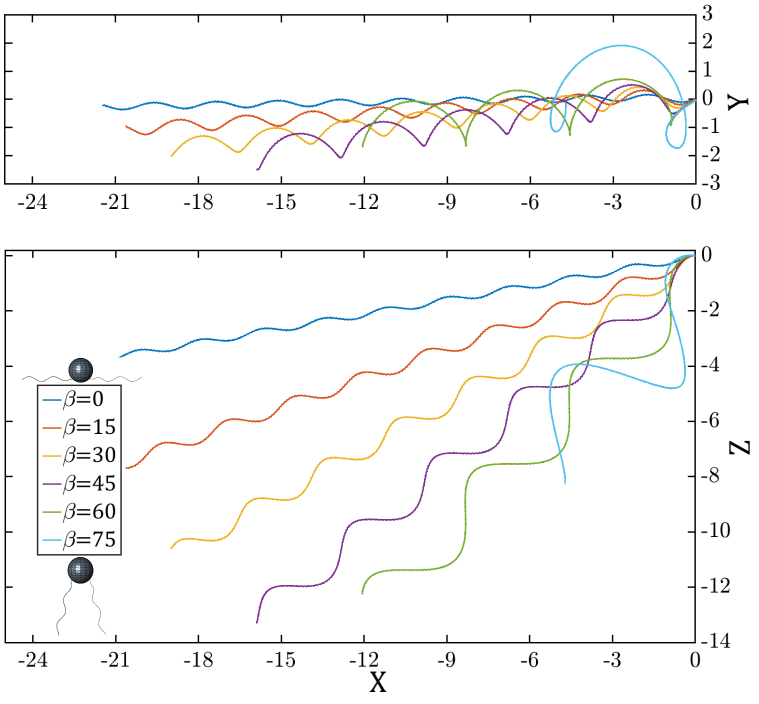

Figure S 5. *The swimming trajectory of the model bacterium projected on XY and XZ planes as function of the flagella orientations (β)(See Movie 4).*

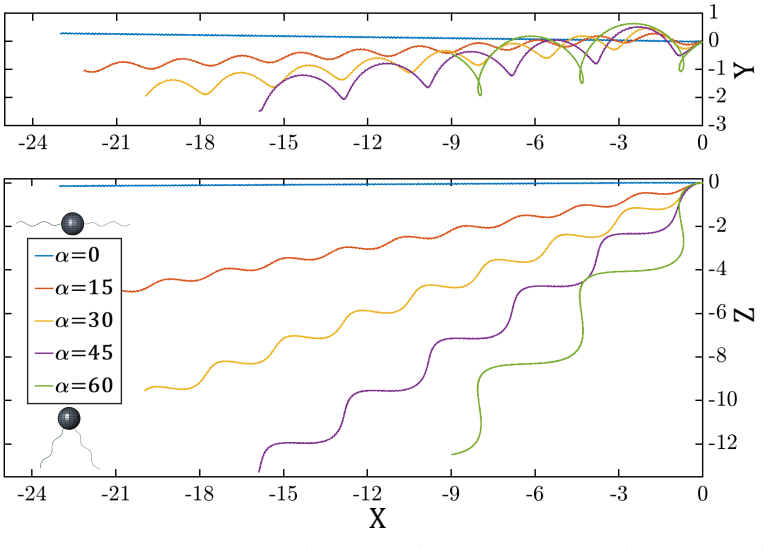

Figure S 6. *The swimming trajectory of the model bacterium projected on XY and XZ planes by changing the flagella places on the cell body (α)(See Movie 5).*

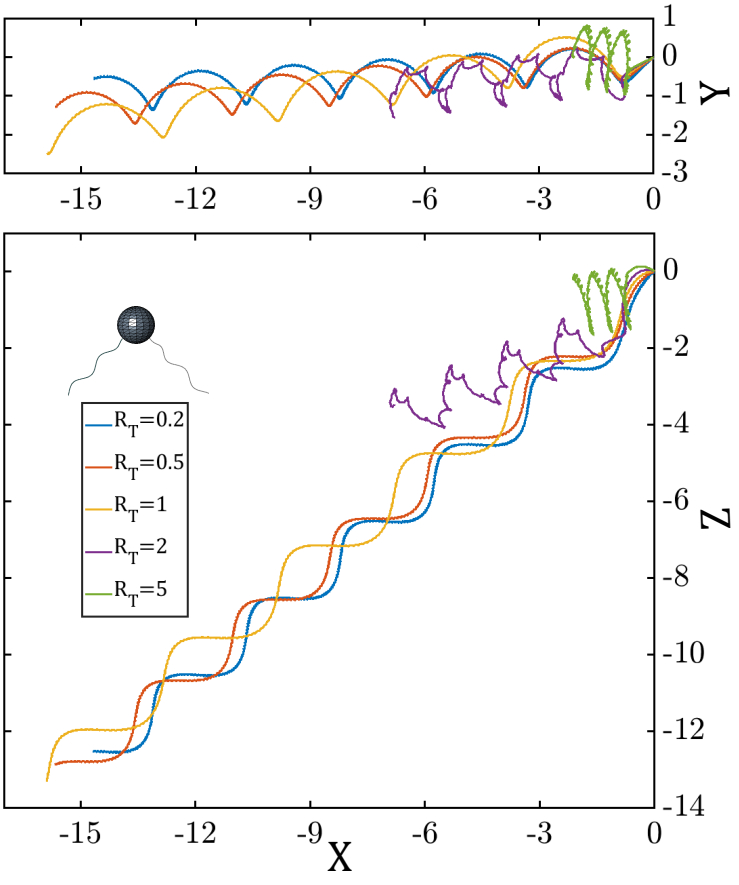

Figure S 7. *The swimming trajectory of the model bacterium projected on XY and XZ planes as function of motor torque ratio* $R_T = |T_1|/|T_2|$ *(See Movie 6).*

References

Jonathan JL Higdon. The hydrodynamics of flagellar propulsion: helical waves. *Journal of Fluid Mechanics*, 94(2):331–351, 1979.

Xianghua Xu and Ali Nadim. Deformation and orientation of an elastic slender body sedimenting in a viscous liquid. *Physics of Fluids*, 6(9):2889–2893, 1994.

RG Cox. The motion of long slender bodies in a viscous fluid part 1. general theory. *Journal of Fluid mechanics*, 44(4):791–810, 1970.